中國機械工程學刊第四十五卷第三期第 303~318 頁(民國一百一十三年)
Journal of the Chinese Society of Mechanical Engineers, Vol.45, No.3, pp303~318 (2024)

# RSM-Based Modelling and Optimization of Performance Measures for WEDM of Inconel 706

Jwala Parshad*, Vivek Aggarwal** and Neelkanth Grover***

**Keywords:** Inconel 706, WEDM machining tool, cutting rate, surface roughness, RSM

## ABSTRACT

Superalloy machining is a significant research concern due to the widespread increase in demand for this category of materials and specific issues with its machining. Due to its easy fabrication, excellent mechanical strength and outstanding high temperature capability, the Inconel 706 superalloy has become more popular than Inconel 718 in the gas turbine industry. Majority of the gas turbine elements have intricate shapes and requires high accuracy, high precision and excellent surface quality. The traditional machining of Inconel 706 superalloy delivers insufficient profile accuracy, low precision and inadequate surface quality. Hence, Response Surface Methodology (RSM)-based experimental investigation of performance measures for WEDM of Inconel 706 has been proposed to optimize the parameters for cutting rate and surface roughness. The existing techniques have not made experimental trials to evaluate the performance of WEDM of Inconel 706. Box and Hunter method which is based on central composite design has been used to design the experiments. It is utilized due to its flexibility, ability to run sequentially, and efficiency in providing the overall experimental error in a minimum number of runs. Single and Multi-response optimization using desirability function approach was performed to get the optimal parameter settings. The propose model was compared with the existing techniques such as grinding wheels (GW), cryogenic holding times (HT) and depth of cut (DOC) on the basis of degrees of freedom (DF), sum of squares (SS), mean square (MS), F-ratio, and PCR%. WEDM machining tool (Electronica Sprint cut ELPULS 40A DLX) along with Metrology Systems' instrument RT-10 Plus has been used to control the process parameter on cutting rate and surface roughness. As a result, the proposed model well optimized the parameters of cutting edge and surface roughness.

*Paper Received September, 2023. Revised February, 2024. Accepted February, 2024. Author for Correspondence: Jwala Parshad*

*Research Scholar, Mechanical Engineering Department, IKG Punjab Technical University Kapurthala (Punjab), jparshad.singla@gmail.com*

***Assistant Professor, Mechanical Engineering Department, IKG Punjab Technical University Kapurthala (Punjab) dr.vivekaggarwal@ptu.ac.in*

****Professor, Mechanical Engineering Department, IKG Punjab Technical University Kapurthala (Punjab) dr.neelkanthgrover@ptu.ac.in*

## INTRODUCTION

Due to the huge growth in demand for this class of materials and specific issues with its machining, super alloy machining is an important research topic. Inconel 706 super alloy has become more popular than Inconel 718 in the gas turbine industry due to its easy fabrication, excellent mechanical strength and outstanding high temperature capability (Wang et al., 2003; Thakur et al., 2009). It also has good resistance to oxidation and corrosion. In the aerospace industry, it is widely used for the production of gas turbine engine parts like turbine discs, blades, combustors and casings, nuclear power plant parts like reactors and pumps, structural parts of spacecraft, casting dies, hot work tools and dies, etc. (Sharman et al., 2006; Thomas et al., 2006). Because of Inconel 706's high toughness, hardness, inclination to work harden, limited heat conductivity and presence of strong abrasive particles, machining by traditional methods is incredibly challenging (Shaw and Nakayama, 1967). In order to machine Inconel 706, non-traditional machining techniques based on chemical, electrochemical, thermal, thermoelectric and mechanical energy are recommended over conventional techniques. With greater precision and accuracy, wire electrical discharge machining (WEDM), a non-traditional thermoelectric process, can be used to cut intricate and complex shapes in all electrically conductive materials used in the tool and die, automotive, aerospace, dental, nuclear, computer, and electronic industries (Kinoshita et al., 1982; Benedict, 1987, Kalpakjian and Schmid, 2008).

WEDM is a well-known process, and the literature (Pandey and Shan, 2010) provides adequate descriptions of how it operates. Material removal rate (also known as cutting rate), surface quality, kerf (cutting breadth), and wire wear rate are the key performance indicators in WEDM. Numerous machining factors, including peak current, pulse-on duration, pulse-off duration, wire tension, wire running speed, spark gap voltage, feed setting, average operating voltage, and dielectric cleansing condition, have an impact on these measurements (Ho et al., 2004; Scott et al., 1991). Due to the quantity and complexity of the process parameters, even a highly competent operator using a cutting-edge WEDM can achieve ideal performance (Williams, and Rajurkar, 1991). The effect of process variables such as pulse on time (Ton), pulse off time (Toff), magnetic field strength (B), and pulse peak current (Ip) on the corner accuracy of the thin-walled shape component of Q235 steel in WEDM need to examine (Manoj et al., 2002].

The impact of the machining factors on wire offset in WEDM was statistically analyzed. It was revealed that the wire offset is greatly influenced by the duration of the sparks and the peak current of the pulses. As these parameters are raised, the discharge energy rises as well, increasing the over-cut magnitude (Dayakar et al., 2019). More material is melted by longer pulses of energy, which spans out around the surface of the machined object and creates bigger globules of debris, increasing surface roughness. The spark gap causes an increase in the discharge voltage. As the electrode wears, the spark gap gradually expands, necessitating a high discharge voltage and making misfire more likely (Ishfaq et al., 2021). The chosen parameters might have detrimental effects, such as wire short circuits and breakage, which would lower production. The link between performance metrics and controllable input factors may be determined in an efficient manner by employing a suitable modelling and optimization technique. To overcome these issues, the novel optimization of parameters for the cutting rate and surface roughness using RSM Inconel 718 with WEDM machining tool has been proposed. The main contribution of this paper are as follows:

❖ To optimize the parameters for cutting rate and surface roughness, RSM-based modeling and optimization of performance measures for WEDM of Inconel 706 has been proposed that optimize parameters (factors) such as pulse-on time (Ton), pulse-off time (Toff), peak current (IP), spark gap voltage (SV), wire running speed (WS), and wire tension (WT) for the cutting rate and surface roughness (response parameters)

❖ To validate the surface roughness and cutting rate model, Inconel 706 is used because it has great thermal and mechanical resistance and performs better in difficult conditions. Also, Box and Hunter method which is based on central composite design has been utilized because of its adaptability, capacity for running in sequential order, and effectiveness in providing the overall experimental error in a limited number of runs.

❖ To control the process parameter for cutting rate and surface roughness, WEDM machining tool (Electronica Sprint cut ELPULS 40A DLX) along with Metrology System’s instrument RT-10 Plus has been used to measure the surface roughness (R) of each machined specimen in micrometers.

Thus, optimization of parameters for the cutting rate and surface roughness using RSM-based model of performance measures for WEDM of Inconel 706 well optimized the parameters of cutting rate and surface roughness. The content of the paper is organized as follows: section 2 describes related works, section 3 provides experimental details, section 4 provides novel solution, the implementation results and its comparison are provided in section 5, finally, section 6 concludes the paper.

## REVIEW OF RELATED WORK

Pawar and Khalkar (2020) used a recently created evolutionary optimization technique to carry out wire-electric discharge machining (wire-EDM) multi-objective optimization. The MOABC method, also known as the multi-objective artificial bee colony algorithm, was created with optimization in mind. The material removal rate and wear ratio were the goals that were taken into consideration in this job, while surface roughness was a restricted. However, it did not process parameters optimization of other advanced and non-traditional manufacturing processes.

Saha et al. (2023) investigated the application of six recently reported metaheuristic optimizers, namely the ant lion optimization (ALO), chimp optimization algorithm (ChoA), moth flame optimization (MFO), spotted hyena optimization (SHO), Harris Hawk optimization algorithm (HHO), and Marine predator algorithm (MPA), to enhance WEDM performances in three WEDM processes. To provide for a fair comparison of the algorithms' performance, this research also included the well-known optimization techniques Particle Swarm Optimization (PSO) and Teaching Learning-Based Optimization (TLBO). The effectiveness of optimum solutions, convergence behavior, and average computing time were some of the metrics used to compare the algorithms. However, need to utilize the HHO optimizer to identify the ideal operating parameters for various industrial processes.

Khatri et al. studied the impact of several process variables on the MRR and surface quality, including powder concentration, pulse on-time, and ultrasonic amplitude. Results from earlier research showed that PMEDM, when compared to conventional EDM, greatly increased the MRR and surface quality of machined MMCs. The flushing and cooling of the machining zone were enhanced by the addition of powder particles to the dielectric fluid and the use of ultrasonic vibrations, minimizing tool wear and increasing machining precision. However, there were some challenges, such as poor surface finish and low material removal rate.

Ahmed et al. (2023) examined the performance of the machining process in relation to the input machining parameters of Electrical Discharge Machining (EDM). Copper was chosen as the electrode material, kerosene as the dielectric medium, and tool steel as the workpiece material. Design of Experiment (DOE) methodology was used in the execution of experimental runs. With a current range of (18 to 24 Ampere), a pulse length ranges of (150 to 200 s), and a pulse-off time range of (25 to 75 s), 20 tests were completed. Based on the output results of the experimental investigation, the influence of the EDM parameter (power supply voltage, discharge current, pulse length, and pulse pause interval) on the responses of the process indicated by surface roughness value (Ra) and Metal Removal rate (MRR). However, there was an impact of input machining parameters of the EDM process on the MRR and Ra.

Boopathi et al. (2022) used a molybdenum wire tool and water-mist wire-cut electrical discharge machining (WEDM), Inconel 600 alloy was cut. The dielectric insulating medium in the plasma zone was created using a small amount of tap water and pressurized air (water-mist). The cutting speed (CS) and surface irregularity (SI) of a novel experimental setup for the near-dry WEDM were predicted utilizing input parameters of the Current (K), Pulse-duration (PD), Pulse-pause time (PP), and Flow Rate (FR) of mixed tap water. It was found that the CS and SI increased with pulse length and current, whereas the CS and SI decreased with PP. Due to the rapid flushing of the debris, the maximum flow rate of tap water resulted in the highest CS and SI. However, further near-dry WEDM research was required to improve the performances.

Farooq et al. (2022) analyzed the four process factors, including servo voltage, flushing pressure, nozzle diameter, and nozzle-workpiece distance. That were examined in connection to geometrical errors (angular and radial deviations), spark gap creation, and arithmetic roughness on Inconel 718. Here, both single-objective and multi-objective process optimization were used in conjunction with detailed statistical and microscopic investigations. However, the impact of flushing qualities had not yet been fully explored.

Abhilash et al. (2022) investigated the effects of discharge energy and debris buildup on wire break failure and elements of surface integrity during Inconel 718 wire EDM, such as surface roughness, subsurface hardness, and geometrical errors. The responses of flatness error, roundness error, and cylindricity error were taken into account while analyzing geometrical accuracy. Based on the wire strength and coatings, four distinct wire electrodes—hard zinc coated brass, half-hard zinc coated brass, hard uncoated brass, and half-hard uncoated brass were taken into consideration for the investigation. The choice of wire electrode had a significant impact on the geometric precision of the machined components. Hard wires with high tensile strength were seen to process the surfaces with the greatest degree of precision. However, during the actual machining, the wire will encounter numerous forces.

Prajapati et al. (2022) examined the best combination of electric discharge machining process characteristics for various alloys, including material removal charge (MRR), device wear price (TWR), and floor roughness. The discharge current, pulse on time, pulse off, arc hole, and obligation cycle were crucial EDM machining factors that had an impact on performance metrics. To achieve the pleasant production circumstances that were essential for industries near to the manufacturing of good products at reduced costs, optimization was one of the tactics utilized in production quarters. However, need to work on parameters for optimization and also suitable techniques for EDM mechanism.

Perumal et al. (2022) used the wire electrical discharge machining (WEDM) technique to manufacture the Ti-6Al-2Sn-4Zr-2Mo alloy. Wire tension, wire feed, and other input parameters were shown to have affected the metal removal rate (MRR) and surface roughness (SR). Using Taguchi's L27 research method, 27 experiments were conducted, and then empirical designing and analysis of variance (ANOVA) were carried out. The Taguchi technique, which was based on the grey relational analysis approach, was employed for process optimization. However, due to insufficient time being elapsed to flush off the removed material, it was allowed to solidify on the molted pool itself during the pulse-off time. This formed the layer and crater surface on the machined region.

Kumarswamy et al. (2023) used Taguchi's L9 orthogonal array, several machining parameters (Pulse on Time, Pulse off Time, and Wire Speed) were optimized in the current experimental research. In this research, presented the welding properties of TIG welding connections made with various currents. To strengthen and enhance the welded connection, the voltages were changed for the number of passes. The goal of the research was to improve the wire cut EDM process parameters for AISI 308 steel and examine the TIG welded connections of the same material's welding properties. The goal of the research was to identify the ideal mix of process variables that will result in the maximum rate of material removal, the lowest rate of wear, and the best tensile qualities of the material. However, welding currents had a significant impact on the welding penetration depth and microstructure of T-welded connections.

From the various analysis it was clear that (Pawar and Khalkar, 2020)] it did not process parameters optimization of other advanced and non-traditional manufacturing processes, (Saha et al., 2023) need to utilize the HHO optimizer to identify the ideal operating parameters for various industrial processes, Khatri there were some challenges, such as poor surface finish and low material removal rate, Ahmed (2023) there was an impact of input machining parameters of the EDM process on the MRR and Ra, (Boopathi et al., 2022) further near-dry WEDM research were required to improve the performances, (Farooq et al., 2022) the impact of flushing qualities had not yet been fully explored, (Abhilash and Chakradhar, 2022) during the actual machining, the wire will encounter numerous forces, (Prajapati et al. 2022) need to work on parameters for optimization and also suitable techniques for EDM mechanism, (Perumal et al., 2022) due to insufficient time being elapsed to flush off the removed material, (Kumarswamy et al., 2023) welding currents had a significant impact on the welding penetration depth and microstructure of T-welded connections.

The extensive review of available literature on WEDM reveals that most of the research work has been carried out on steels and some other materials/composites. However, as far as Inconel 706 is concerned, comparatively less research has been done. Inconel 706 has a vast range of applications, but despite having such a large application domain, relatively fewer papers have been reported on the use of WEDM for machining Inconel 706. This may be due to the reasons that Inconel 706, a difficult-to-cut material, has typical characteristics like presence of hard abrasive carbides in the microstructure, low thermal conductivity and specific heat, and high cutting temperature. Therefore, the choice of correct parametric combination of WEDM process for this material becomes a challenging task. There is no acceptable analytical model for WEDM process due to the presence of a large number of variables and complicated stochastic process mechanism which necessitates the use of empirical and experimental studies of WEDM process with the goal of achieving mathematical models to enhance the process performance.

It is also observed that the available research work that has been carried out for WEDM of Inconel 706 investigated the impact of a limited number of process parameters. The effect of spark gap voltage on performance is studied by very few researchers, although it may play an influential role in WEDM process. Therefore, in this research work, WEDM of Inconel 706 has been carried out in order to develop the empirical models for investigating the impact of various process parameters including spark gap voltage on performance measures to obtain the optimum machining conditions. The present work is largely focused on machining of Inconel 706 with reference to the applications like manufacturing of extrusion dies and containers, hot work tools and dies, casting dies, food processing equipment, etc. The actual values of input process parameters have been considered to make the models more realistic and useful.

## EXPERIMENTATION

The details such as work material, experimental set-up and measuring instruments, selection of parameters, design of experiments and reproducibility are given in this section.

### 3.1 Work-piece material

In recent years, Inconel 706 has replaced Inconel 718 as the preferred superalloy for turbine wheel applications. Inconel 706, a nickel-based superalloy finds extensive usage in the nuclear power industry, rocket engines, extrusion dies, hot work tools, medical devices, and casting dies etc. Unlike Inconel 718, Inconel 706 don’t contain molybdenum in order to enhance its forgeability. Due to its tendency to get work-harden, Inconel 706 is extremely difficult to machine using traditional methods. The material was procured in 25 mm × 25 mm × 600 mm size. Table 1 displays the elemental details of the selected work material provided by the supplier and confirmed by an electron probe micro-analyzer (EPMA).

Table 1: Chemical composition of Inconel 718

| Element | Ni | Fe | Cr | Nb | Mn | C | Co | Al | Si | Ti | Cu |
|---|---|---|---|---|---|---|---|---|---|---|---|
| Weight % | 40.38 | 38.08 | 15.37 | 2.87 | 0.26 | 0.042 | 0.43 | 0.23 | 0.18 | 1.89 | 0.11 |

### 3.2 Machine tool and apparatus

In this research work, an Electronica Sprint cut ELPULS 40A DLX, WEDM machine tool has been used for all investigations. The experiments are designed to investigate the effects of various process parameters that are under control on performance indicators such as cutting rate and surface roughness. The cutting rate (in mm/min) is indicated on the machine's control panel. As compared to other wire materials, such as plain and diffused brass wires, a zinc-coated brass wire (0.25 mm) is selected based on minimum breakage frequency. Surface roughness (in micrometers) for each specimen, was determined by Metrology System's RT-10 Plus roughness tester. Mean value (Ra) of roughness was noted as response parameter. The measurement has been chosen using a sampling length of 2.5 mm in five increments.

### 3.3 Input Parameters and their levels

A set of experiments have been performed as per design of experiments. The impact of several process parameters (factors) such as pulse-on time (Ton), pulse-off time (Toff), peak current (IP), spark gap voltage (SV), wire running speed (WS), and wire tension (WT) on performance measures such as cutting rate and surface roughness has been studied. The independent parameters and their range have been chosen in accordance with the available literature, pilot tests, machine capabilities and manufacturer's instructions. Table 2 gives the set of independent process parameters, their symbols, and their levels in coded and actual values. Table 3 shows the values of the constant parameters.

### 3.4 Experimental design

The experimental design, the development of mathematical relationship between input parameters and output response (cutting rate and surface roughness), and the analysis of the effects of process parameters on these responses have been carried out using the central composite design approach of response surface methodology. The experimentation along with regression analysis facilitates the modeling of the desired response in terms of several input process parameters. The experiments are designed to allow estimation of interaction and even quadratic effects and, thus, provides an idea of the local shape of the response surface. Hence, it is termed as response surface method design. In RSM, a relationship between the desired response and the independent input parameters can be represented by equation (1)

$$Y_1 = f(X_1, X_2, X_3, \, ..X_k) \pm \varepsilon \quad (1)$$

Table 2: Independent process parameter

| Input Parameter (symbol) | Definition | Unit | Notation | Levels | | | | |
|---|---|---|---|---|---|---|---|---|
| | | | | 1.56 | -1.56 | -1 | 0 | 1 |
| Pulse-on time (A) | Time-duration for which current is flowing in each cycle | µs | $T_{on}$ | 0.45 | 0.65 | 1.0 | 1.35 | 1.55 |
| Pulse-off time (B) | Time-interval between two Consecutive sparks | µs | $T_{off}$ | 10 | 16 | 27 | 38 | 44 |
| Peak current (C) | Maximum value of current flowing through electrodes given pulse | A | *IP* | 80 | 105 | 150 | 195 | 220 |
| Spark gap (D) | Voltage difference between wire electrode and workpiece during erosion | V | *SV* | 18 | 16 | 27 | 38 | 44 |
| wire running speed (E) | Rate at which wire moves through wire guides | m/min | *WS* | 2 | 4 | 7 | 10 | 12 |
| Wire tension (F) | Gram-equivalent load to keep the continuously fed wire under tension | g | *WT* | 400 | 600 | 1000 | 1400 | 1600 |

Table 3: Constant input parameters and their values

| Parameter | Description or value |
|---|---|
| Wire material | Zinc-coated brass wire |
| Wire diameter | 0.25 mm |
| Workpiece material | Inconel 706 |
| Dielectric fluid | Deionized water |
| Conductivity of dielectric fluid | 20 mho |
| Flushing pressure | 15 kg/cm$^2$ |
| Pulse peak voltage | 110 V DC |
| Servo feed | 2100 units |
| Machining width | 25 mm |
| Machining height | 25 mm |
| Thickness | 15 mm |

Table 4: Thermal properties and their values

| Thermal properties | Values |
|---|---|
| Thermal conductivity | 12.5 W/mK |
| Thermal expansion co-efficient | 13.46 µm/m°C |
| Specific Heat Capacity | 0.45 J/g°C. |
| Melting range | 1334–1371 °C |

where $Y$, is the desired response, f is the response function and $X_1, X_2, X_3, \, ..X_k$ are independent input process parameters. The fitting error, $\varepsilon$ also called residual, measures the experimental errors. The approximation of response function has been proposed using the second-order polynomial regression model, also called quadratic model. The quadratic model for input process parameters can be expressed by the following equation (2)

$$y_I = b_o + \sum_{i=1}^{k} b_i x_i + \sum_{i=1}^{k} b_{ii} \, x_i{}^2 + \sum\sum_{i<j}^{k} b_{ij} \, x_i x_j + \varepsilon \quad (2)$$

whereby $b_o$ is a constant and $b_i, b_{ii}$ and $b_{ij}$ represent the coefficients of linear, quadratic, and cross product terms respectively. The variable $x$ corresponds to the process parameter under study. The response surface, $y$ contains linear terms, squared terms, and interaction terms.

In central composite design (CCD) each factor is varied at five levels $(-\alpha, -1, 0, 1, \alpha)$ for developing a second-order model as given in equation (2). Fifty-two sets of experiments have been conducted according to the CCD of response surface methods using half replication for six factors with $\alpha = 1.565$ ($\alpha$=$k^{1/4}$). When the number of factors (k) is five or greater. The 52 trials consist of 32 factorial points (run 1 to 32), 12 axial points to form a CCD with a 1.565 for estimation of curvature (run 33 to 44), and eight center points (run 45 to 52) at zero level for replication to estimate pure error. The experimental runs are randomized to prevent human biases. The design was generated and analyzed using Design-Expert software (Stat-Ease, Inc., Minneapolis, v 8.0.6.1). Table 5 shows the set of process parameters and corresponding response values (mean) obtained from experimentation.

### 3.5. Reproducibility

Eight experiments using CCD approach are conducted at the centre of the input variables to test the process' repeatability. The outcomes of the experimental runs (45 to 52) are also displayed separately in Table 6. The percentage error (Eq. 3) illustrates the response parameters' variability concerning their average value (the sum of all terms divided by the total number of terms).

$$Percentage\ error = \left(\frac{Average\ value - Experimental\ value}{Average\ value}\right) \times 100 \quad (3)$$

Table 5: Experimental design matrix with set of input parameters and response parameters

| Standard order | Run order | Location | Process parameters | | | | | | Response parameters | |
|---|---|---|---|---|---|---|---|---|---|---|
| | | | $T_{on}$ (μs) | $T_{off}$ (μs) | *IP* (A) | *SV* (V) | *WS* (m/min) | *WT* (g) | Cutting rate (mm/min) | Surface roughness (μm) |
| 1 | 5 | Factorial | 0.65 | 16 | 105 | 30 | 4 | 600 | 1.54 | 2.26 |
| 2 | 42 | Factorial | 1.35 | 16 | 105 | 30 | 4 | 1400 | 2.54 | 3.29 |
| 3 | 39 | Factorial | 0.65 | 38 | 105 | 30 | 4 | 1400 | 0.94 | 2.32 |
| 4 | 47 | Factorial | 1.35 | 38 | 105 | 30 | 4 | 600 | 1.61 | 3.05 |
| 5 | 2 | Factorial | 0.65 | 16 | 195 | 30 | 4 | 1400 | 1.62 | 2.39 |
| 6 | 14 | Factorial | 1.35 | 16 | 195 | 30 | 4 | 600 | 2.62 | 3.28 |
| 7 | 49 | Factorial | 0.65 | 38 | 195 | 30 | 4 | 600 | 1.33 | 2.38 |
| 8 | 33 | Factorial | 1.35 | 38 | 195 | 30 | 4 | 1400 | 1.82 | 3.1 |
| 9 | 29 | Factorial | 0.65 | 16 | 105 | 70 | 4 | 1400 | 0.8 | 1.68 |
| 10 | 20 | Factorial | 1.35 | 16 | 105 | 70 | 4 | 600 | 1.3 | 2.51 |
| 11 | 18 | Factorial | 0.65 | 38 | 105 | 70 | 4 | 600 | 0.46 | 1.63 |
| 12 | 35 | Factorial | 1.35 | 38 | 105 | 70 | 4 | 1400 | 0.79 | 2.3 |
| 13 | 34 | Factorial | 0.65 | 16 | 195 | 70 | 4 | 600 | 0.98 | 1.64 |
| 14 | 12 | Factorial | 1.35 | 16 | 195 | 70 | 4 | 1400 | 1.36 | 3 |
| 15 | 38 | Factorial | 0.65 | 38 | 195 | 70 | 4 | 1400 | 0.54 | 1.82 |
| 16 | 19 | Factorial | 1.35 | 38 | 195 | 70 | 4 | 600 | 1.08 | 3.1 |
| 17 | 30 | Factorial | 0.65 | 16 | 105 | 30 | 10 | 1400 | 1.56 | 2.37 |
| 18 | 15 | Factorial | 1.35 | 16 | 105 | 30 | 10 | 600 | 2.57 | 3.11 |
| 19 | 32 | Factorial | 0.65 | 38 | 105 | 30 | 10 | 600 | 0.92 | 2.21 |
| 20 | 28 | Factorial | 1.35 | 38 | 105 | 30 | 10 | 1400 | 1.63 | 3.17 |
| 21 | 25 | Factorial | 0.65 | 16 | 195 | 30 | 10 | 600 | 1.99 | 2.46 |
| 22 | 9 | Factorial | 1.35 | 16 | 195 | 30 | 10 | 1400 | 2.64 | 3.13 |
| 23 | 43 | Factorial | 0.65 | 38 | 195 | 30 | 10 | 1400 | 1.31 | 2.27 |
| 24 | 21 | Factorial | 1.35 | 38 | 195 | 30 | 10 | 600 | 1.81 | 3.31 |
| 25 | 10 | Factorial | 0.65 | 16 | 105 | 70 | 10 | 600 | 0.82 | 1.6 |
| 26 | 52 | Factorial | 1.35 | 16 | 105 | 70 | 10 | 1400 | 1.31 | 2.62 |
| 27 | 51 | Factorial | 0.65 | 38 | 105 | 70 | 10 | 1400 | 0.48 | 1.68 |
| 28 | 7 | Factorial | 1.35 | 38 | 105 | 70 | 10 | 600 | 0.77 | 2.22 |
| 29 | 44 | Factorial | 0.65 | 16 | 195 | 70 | 10 | 1400 | 1.01 | 1.71 |
| 30 | 8 | Factorial | 1.35 | 16 | 195 | 70 | 10 | 600 | 1.41 | 3.01 |
| 31 | 6 | Factorial | 0.65 | 38 | 195 | 70 | 10 | 600 | 0.51 | 1.64 |
| *32* | 50 | Factorial | 1.35 | 38 | 195 | 70 | 10 | 1400 | 1.08 | 2.9 |
| *33* | 36 | Axial | 0.45 | 27 | 150 | 50 | 7 | 1000 | 0.89 | 1.54 |
| *34* | 37 | Axial | 1.55 | 27 | 150 | 50 | 7 | 1000 | 1.84 | 3.42 |

| | | | | | | | | | | |
|---|---|---|---|---|---|---|---|---|---|---|
| *35* | 11 | Axial | 1 | 10 | 150 | 50 | 7 | 1000 | 1.83 | 2.96 |
| 36 | 22 | Axial | 1 | 44 | 150 | 50 | 7 | 1000 | 0.92 | 2.36 |
| 37 | 45 | Axial | 1 | 27 | 80 | 50 | 7 | 1000 | 1.23 | 1.74 |
| 38 | 40 | Axial | 1 | 27 | 220 | 50 | 7 | 1000 | 1.51 | 2.54 |
| 39 | 48 | Axial | 1 | 27 | 150 | 18 | 7 | 1000 | 2.16 | 2.89 |
| 40 | 46 | Axial | 1 | 27 | 150 | 82 | 7 | 1000 | 0.75 | 1.86 |
| 41 | 27 | Axial | 1 | 27 | 150 | 50 | 2 | 1000 | 1.88 | 2.63 |
| 42 | 13 | Axial | 1 | 27 | 150 | 50 | 12 | 1000 | 1.61 | 2.66 |
| 43 | 17 | Axial | 1 | 27 | 150 | 50 | 7 | 400 | 1.92 | 2.46 |
| 44 | 4 | Axial | 1 | 27 | 150 | 50 | 7 | 1600 | 1.88 | 2.52 |
| 45 | 16 | Center | 1 | 27 | 150 | 50 | 7 | 1000 | 1.78 | 2.68 |
| 46 | 24 | Center | 1 | 27 | 150 | 50 | 7 | 1000 | 1.79 | 2.48 |
| 47 | 31 | Center | 1 | 27 | 150 | 50 | 7 | 1000 | 1.75 | 2.79 |
| 48 | 41 | Center | 1 | 27 | 150 | 50 | 7 | 1000 | 1.88 | 2.66 |
| 49 | 26 | Center | 1 | 27 | 150 | 50 | 7 | 1000 | 1.76 | 2.61 |
| 50 | 3 | Center | 1 | 27 | 150 | 50 | 7 | 1000 | 1.87 | 2.75 |
| 51 | 23 | Center | 1 | 27 | 150 | 50 | 7 | 1000 | 1.81 | 2.6 |
| 52 | 1 | Center | 1 | 27 | 150 | 50 | 7 | 1000 | 1.73 | 2.54 |

The results in Table 6 show that the surface roughness and cutting rate are replicated within the allowed range of 5%. In order to illustrate the variability of the response parameters over a series of repeated experiments, the values of experimental standard deviation and standard uncertainty have also been determined. Cutting rate and surface roughness's standard uncertainties, which are determined as 1.98 and 2.54%, respectively fall well within the permissible range.

Table 6: Reproducibility and percentage error in cutting rate and surface roughness

| $T_{on}$ (μs) | $T_{off}$ (μs) | *IP* (A) | *SV* (V) | *WS* (m/min) | *WT* (g) | Cutting rate (mm/min) | | Surface roughness (μm) | |
|---|---|---|---|---|---|---|---|---|---|
| | | | | | | Experimental Value | % Error | Experimental Value | % Error |
| 1 | 27 | 150 | 50 | 7 | 1000 | 1.76 | 1.67 | 2.68 | -7.33 |
| 1 | 27 | 150 | 50 | 7 | 1000 | 1.79 | 0 | 2.48 | 0.68 |
| 1 | 27 | 150 | 50 | 7 | 1000 | 1.75 | 2.23 | 2.79 | -11.7 |
| 1 | 27 | 150 | 50 | 7 | 1000 | 1.88 | -5.02 | 2.66 | -6.53 |
| 1 | 27 | 150 | 50 | 7 | 1000 | 1.76 | 1.67 | 2.61 | -4.53 |
| 1 | 27 | 150 | 50 | 7 | 1000 | 1.87 | -4.46 | 2.75 | -10.1 |
| 1 | 27 | 150 | 50 | 7 | 1000 | 1.81 | -1.11 | 2.6 | -4.12 |
| 1 | 27 | 150 | 50 | 7 | 1000 | 1.73 | 3.35 | 2.54 | -1.72 |

## DEVELOPMENT OF REGRESSION MODELS AND OPTIMIZATION

It is challenging to develop an analytical model for the WEDM process based on its physics because of its complexity and stochastic character. In order to discover the mathematical relationship between process parameters and performance measure based on the experimental findings, a multi-variable regression equation (model) using response surface methodology has been developed for each response. The findings of the selected model are then statistically analyzed using analysis of variance (ANOVA). Significant parameters are identified and their interaction effects on the response parameters are analyzed using response surface graphs.

### 4.1 Regression model and ANOVA for Cutting Rate

Design-Expert software has been used to analyze the experimental data for cutting rate (Table 5) Three tests—the sequential model sum of squares, the lack-of-fit test, and the model summary statistics— are performed to determine the adequacy of the model. The fit statistics of three tests suggests that the quadratic model is adequate. According to the ANOVA results several insignificant terms are present in the quadratic model. The model is then improved by eliminating insignificant terms using backward elimination. Appendix-I gives the outcomes of the pooled ANOVA after backward elimination for cutting rate.

The residuals' normal probability plot (figure 1a) reveals that 98% of the residuals are within three sigma limits and lie on a straight line So, the errors are normally distributed. Figure 1b shows that the actual values are close to those predicted by the model. It can be concluded that the ANOVA results shown in Appendix-I are accurate and reliable.

The "model" mean square divided by the "residual" mean square yields the model F-value. The F-value for each factor term is evaluated in similar manner. So, the variance of the model (or term) is compared with that of residuals. If this ratio is near to one the likelihood that the model (or factor terms) will significantly affect the response term is lower. If the computed F-value (at a selected confidence level) is higher than the tabulated F-value at equal confidence level, then that source of variation may be significant. The confidence level for this study is set at 95%. The model F-value of 139.90 with P-value < 0.0500 implies that the model is significant for cutting rate. There is only a 0.01% chance that an F-value this large could occur due to noise. P-values less than 0.0500 indicate that model terms are significant. In this case A, B, C, D, AB, AD, BD, $A^2$, $B^2$, $C^2$, $D^2$, $F^2$ are significant model terms for cutting rate with their percentage contribution of 20.87, 18.65, 2.11, 43.78, 0.35, 1.26, 1.17, 1.63, 1.53, 1.58, 0.86, and 0.6% respectively. These percentage values are calculated from Appendix-I by taking the ratio of "individual term" sum of squares and "model" sum of squares. P-value > 0.0500 indicate that the model terms are insignificant.

The lack of fit is not significant and lack of fit F-value of 3.35 implies there is a 5.08% chance that a lack of fit F-value this large could occur due to noise. Therefore, the model for cutting rate is acceptable.

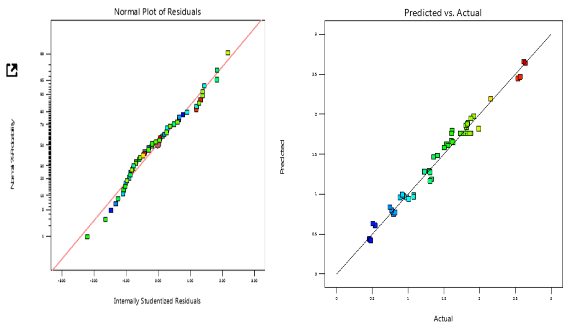


Figure 1: a Normal probability plot of residuals. b Plot of predicted vs. actual response for Cutting rate

Further, the determination coefficient ($R^2$), measured as the ratio of explained variance to total variation is determined to confirm whether the fine-tuned models accurately describe the experimental data. The response model exhibits better data fit and less discrepancy between projected and actual values as $R^2$ gets closer to unity. The $R^2$ value equal to 0.9795 (from Appendix-I) indicate that model can justify the variation in the cutting rate up to a degree of 97.95%. The high values of the determination coefficient indicate that the proposed model adequately represent the process. The Predicted $R^2$ (0.9608) and the Adj $R^2$ (0.9725) are also in good agreement.

The coefficient of variation (CV) of the model is defined as the ratio of the standard deviation to the mean. The value of CV% equal to 6.37, shows that the experiments conducted were precise and reliable. Additionally, the signal-to-noise ratio is measured with the adequate precision. A ratio of more than 4 is generally preferred. The model's adequate precision was 46.29, which is significantly higher than the preferred value and indicates that signal is adequate for the model. As a result, model for cutting rate may be employed to explore the design space and forecast the cutting rate within the constraints of investigated factors.

The finally accepted second-order polynomial empirical model for cutting rate is given in Eq. (4)

$$Cutting\ rate = -1.45023 + 3.88921 \times T_{on} + 0.027986 \times T_{off} + 0.022150 \times IP + 0.004260 \times SV - 0.001152 \times WT - 0.010888 \times T_{on} \times T_{off} - 0.011004 \times T_{on} \times IP - +0.000342 \times T_{off} \times SV - 1.09772 \times T^2{}_{on} - 0.001114 \times T^2{}_{off} - 0.000067 \times IP^2 - 0.000236 \times SV^2 + 5.63722\,E - 07 \times WT2 \quad (4)$$

The coefficients in the above equation have been determined based on analysis of the experimental data (in Table 5) by using Design-Expert software.

**4.2 Regression model and ANOVA for Surface Roughness**

Appendix-II gives the outcomes of the pooled ANNOVA after backward elimination for surface roughness.

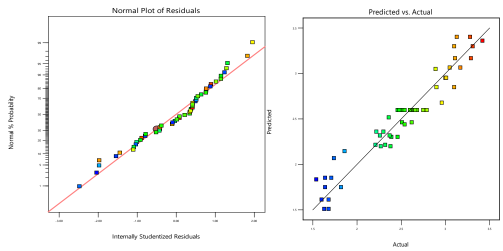


Figure 2 a Normal probability plot of residuals. b Plot of predicted vs. actual response for surface roughness

The residuals' normal probability plot (figure 2a) reveals that 98% of the residuals are within three sigma limits and lie on a straight line So, the errors are normally distributed. Figure 2b shows that the actual values are close to those predicted by the model. It can be concluded that the ANOVA results shown in Appendix-II are accurate and reliable.

If the computed F-value (at a selected confidence level) is higher than the tabulated F-value at selected confidence level, then that source of variation may be significant. The confidence level for this study is set at 95%. The model F-value of 90.54 with P-value<0.0001 implies that the model is significant for surface roughness. There is only a 0.01% chance that an F-value this large could occur due to noise. P-values less than 0.0500 indicate that model terms are significant. In the present case the model terms A, B, C, D. AC, AD, CD, and $C^2$ are significant for surface roughness with their percentage contribution of 63.50, 0.78, 3.49, 26.73, 0.62, 0.59, 1.01 and 3.28 respectively. These percentage values are calculated from Appendix-II by taking the ratio of "individual term" sum of squares and "model" sum of squares. P-value>0.0500 indicate that the model terms are insignificant.

The lack of fit is not significant and lack of fit F-value of 2.16 implies there is a 14.47% chance that a lack of fit F-value this large could occur due to noise. Therefore, the model for surface roughness is acceptable.

Further, the determination coefficient ($R^2$) value equal to 0.9440 (from Appendix-II) indicates that the model can justify the variation in the surface roughness up to a degree of 94.40%. The high values of the determination coefficient indicate that the proposed model adequately represent the process. The Predicted $R^2$ (0.9170) and the Adj $R^2$ (0.9335) are also in good agreement.

The value of coefficient of variation (CV) equal to 6.37, shows that the experiments conducted were precise and reliable. Further, the signal-to-noise ratio is measured with the adequate precision. A ratio of more than 4 is generally preferred. The model's adequate precision was 34.11, which is significantly higher than the preferred value and indicates that signal is adequate for the model. As a result, model for surface roughness may be employed to navigate the design space and forecast the surface roughness within the constraints of investigated factors.

The finally accepted second-order polynomial empirical model for surface roughness is given in Eq. (5)

$$Surface\ roughness = 1.32684 + 0.560118 \times T_{on} - 0.005187 \times T_{off} + 0.020275 \times IP - 0.034630 \times SV + 0.003420 \times T_{on} \times IP + 0.007307 \times T_{on} \times SV + 0.000075 \times IP \times SV - 0.000083 \times IP^2 \quad (5)$$

The coefficients in the above equation have been determined based on analysis of the experimental data (in Table 5) by using Design-Expert software.

### 4.3 Models Validation

A set of seven experiments with parameter settings within the range of the chosen parameters have been carried out so as to validate the models for cutting rate and surface roughness. The results of the experiments conducted are given in Table 7. The following Eq. (6) calculate the prediction error (%) and is tabulated in Table 7:

$$Prediction\ error\ (\%) = \left(\frac{experimental\ result - predicted\ result}{experimemntal\ result}\right) \times 100 \quad (6)$$

The prediction errors are within the acceptable range of ±5% consequently, it is possible to accept the models for cutting rate and surface roughness as an accurate representation of the experimental findings.

Table 7: Results of validation experiments for cutting rate and surface roughness

| $T_{on}$ (μs) | $T_{off}$ (μs) | $IP$ (A) | $SV$ (V) | $WS$ (m/min) | $WT$ (g) | Cutting rate (mm/min) | | | Surface roughness (μm) | | |
|---|---|---|---|---|---|---|---|---|---|---|---|
| | | | | | | Experimental Value | Predicted value | Prediction error (%) | Experimental Value | Predicted value | Prediction error (%) |
| 1 | 26 | 160 | 45 | 7 | 900 | 1.86 | 1.92 | -3.22 | 2.81 | 2.73 | 2.84 |
| 1.2 | 24 | 120 | 55 | 6 | 700 | 1.86 | 1.79 | 3.76 | 2.62 | 2.68 | -2.29 |
| 0.6 | 18 | 100 | 35 | 5 | 500 | 1.54 | 1.48 | 3.89 | 2.11 | 2.18 | -3.31 |
| 0.8 | 14 | 170 | 40 | 8 | 1100 | 1.86 | 1.90 | -2.15 | 2.65 | 2.57 | 3.01 |
| 1.3 | 32 | 140 | 70 | 9 | 1300 | 1.28 | 1.24 | 3.12 | 2.63 | 2.70 | -2.66 |
| 1.4 | 38 | 150 | 80 | 11 | 1500 | 0.74 | 0.76 | -2.70 | 2.83 | 2.75 | 2.82 |

### 4.4 Single and Multi-response optimization

One of the frequently employed strategies for solving problems related to the optimization of both single and multi-objective is the desirability function approach. This method converts an estimated response into a scale-free value known as desirability. The preferred range is between 0 to 1 (from least desirable to most desired, respectively). The input parameter settings corresponding to the most desirable response are regarded as the ideal parameter conditions. This strategy has been employed by several writers for manufacturing applications, and the entire process has been accurately documented and presented.

In this work, the Design-Expert software's optimization module has been used to identify the input parameter combinations—namely, pulse-on time, pulse-off time, peak current, spark gap voltage, wire running speed, and wire tension, compliance with the criteria placed on each response and process parameter. The optimization procedure looks for the ideal values of cutting rate and surface roughness, by increasing cutting rate while decreasing surface roughness both simultaneously and separately. Table 8 lists the constraints for the input and response parameters. The optimum values of operating input parameters and the relevant responses have been evaluated with the help of software and are recorded in Table 8. For multi-response optimization, both responses were taken into account and given equal weightage whereas to carry out single-response optimization the other response was ignored.

Table 8: values for input and response parameter

| Input parameters | | | |
|---|---|---|---|
| Parameters | Goal | Lower limit | Upper limit |
| Pulse-on time (μs) | In range | 0.45 | 1.55 |
| Pulse-off time (μs) | In range | 10 | 44 |
| Peak current (A) | In range | 80 | 220 |
| Spark gap (V) | In range | 18 | 82 |
| Wire running speed (m/min) | In range | 2 | 12 |
| Wire tension (g) | In range | 400 | 1600 |
| Response results | | | |
| Cutting rate (mm/min) | Maximize | 0.46 | 2.64 |
| Surface roughness (μm) | Minimize | 1.54 | 3.50 |

Table 9: Optimal combinations of input parameters for single and multi-response optimization and comparison with results

| Type of Optimization | Objective | Optimum parameters | | | | | | Response (Predicted) | Response (Experimental) | Desirability |
|---|---|---|---|---|---|---|---|---|---|---|
| | | $T_{on}$ (μs) | $T_{off}$ (μs) | *IP* (A) | *SV* (V) | *WS* (m/min) | *WT* (g) | | | |
| Single response | To maximize cutting rate | 1.15 | 17 | 190 | 18 | 12 | 400 | 2.80 | 2.72 | 1.0 |
| Single response | To minimize surface roughness | 0.65 | 30 | 85 | 62 | 10 | 500 | 1.39 | 1.45 | 1.0 |
| Multi-response | To maximize cutting rate and minimize surface roughness | 0.75 | 17 | 220 | 36 | 3 | 400 | 1.88 mm/min and 2.21 μm | 1.80 mm/min and 2.30 μm | 0.654 |

In comparison to the results reported in the literature, the results shown in Table 9 show an impressive improvement in cutting rate and surface roughness for Inconel 706 cut by WEDM. Confirmatory tests have been conducted to validate the best outcomes. The response parameters found experimentally (Table 9) are very close to the predicted values.

# PERFORMANCE ANALYSIS AND DISCUSSION

Cutting rate and surface roughness are critical performance indicators in a WEDM process because of their significant impact on the industrial economy and surface integrity. In this section, the influence of selected process parameters as well as their interactions on the performance measures of WEDM of Inconel 706 have been thoroughly discussed using perturbation plots and three-dimensional (3D) response curves.

The influence of optimal parameters, specifically pulse-on time and spark gap voltage, are able to be explained theoretically and visually. The pulse-on time is essential because it determines the duration of the electrical discharge, which influences the amount of energy delivered to the workpiece. A longer pulse-on time allows for more discharge energy, which improves material removal. This is visible in the photomicrographs, where longer pulse-on times show more efficient material removal. Spark gap voltage, instead, is critical in controlling the gap between the wire electrode and the workpiece. A higher spark gap voltage expands the gap, increasing dielectric strength and decreasing discharge current. Theoretical analysis backs this up by showing that a larger gap results in less melting and evaporation of the work material. This explanation is supplemented by photomicrographs, which show smoother surfaces at lower spark gap voltages.

## 5.1 Effect of individual parameters on performance measures

The perturbation plot in Figure 3a compares the effects of important process factors on the cutting rate of Inconel 706 cut by WEDM. The middle value (coded value 0) of all factors is selected as default reference point by Design-Expert software. While relatively flat lines for and

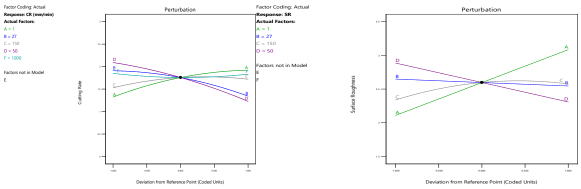

Figure 3 a Perturbation plot for cutting rate b Perturbation plot for surface roughness

peak current (C) and wire tension (F) reveal relatively less sensitivity to cutting rate, a steep slope for pulse-on time (A), pulse-off time (B), and spark gap voltage (D) shows that the cutting rate is quite sensitive to these parameters. While describing the interaction effects, the causes of these trends were covered.

The perturbation plot in Figure 3b compares the effects of important process factors on the surface roughness of Inconel 706 cut by WEDM. A relatively flat line for peak current (C) and pulse-off time (B) indicates that surface roughness is less sensitive to these variables, but a steep slope for pulse-on time (A) and spark gap voltage (D) indicates that these variables are extremely sensitive to surface roughness. While describing the interaction effects, the causes of these trends were covered.

### 5.2 Micrographs of the WEDM machined surfaces

Microstructural images of the WEDM machined surface were captured using a scanning electron microscope at a magnification of 1000. The microscopic images of WEDM-processed Inconel 706, were captured at a 15 kV acceleration voltage. Secondary electron images (SEI) were captured using a 10 µm aperture. The microstructure of the WED machined surface shows craters and micro holes, but no micro cracks were observed due to the high toughness of Inconel 706.

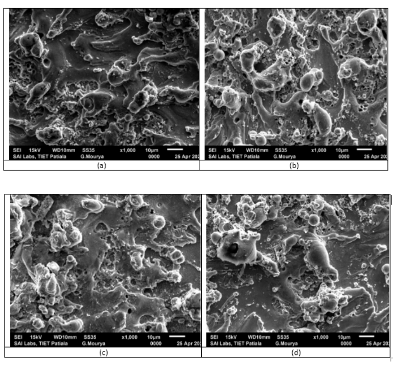

Figure 4: Micrographs of the WEDM machined surfaces at a) Lowest pulse-on time= 0.45 µs (Run order-36), b) Highest pulse-on time=1.55 µs (Run order-37), c) Lowest pulse-off time= 10 µs (Run order-11) and d) Highest pulse-off time= 44 µs (Run order-22)

The SEM micrograph Figure 4(a-d) shows that the surface topography of the machined surface improves under optimized conditions. A Melting and evaporation of work material occurred during WEDM machining, and the material was removed in a spherical shape, causing crater and crack formation. The density of cracks is determined by the discharge energy and the thermal properties of the work material. Because at the highest pulse-on time 1.15 µs, more energy transfers towards the work surface, and more material melts and evaporates from the work piece's surface. When the pulse-on time is low, less discharge energy is transferred to the work surface and less melted material is blasted from the work surface by dielectric pressure.

### 5.3 Interactions of parameters and performance measures

#### 5.3.1 Effect of parametric interactions on cutting rate

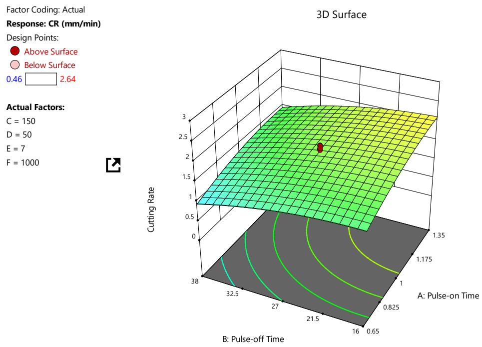


Figure 5: Response surface showing the interactive effect of pulse-on time and pulse-off time on the cutting rate at peak current=150 A, spark gap voltage= 50 V, wire running speed =7.0 m/min, and wire tension=1000 g

Figure 5 depicts the effect of pulse-on and pulse-off time on cutting rate while keeping all other input parameters constant. The observed trend shows that the cutting rate increases as the pulse-on time increases. This phenomenon is attributed to the fact that the discharge energy, represented by the area under the discharge current curve, has a significant influence on material removal from the work specimen rather than being simply the product of pulse-on time and peak current. Furthermore, as the pulse-off time increases, the cutting rate decreases. This is due to the longer pulse-off time resulting in fewer discharges within a given timeframe, resulting in fewer particles dislodging near the work material's surface. It is worth noting that the effect of pulse-on time on cutting rate is more pronounced at low pulse-off times than at high pulse-off times. The best cutting rate is achieved with a pulse-on time of 1.35 seconds and a pulse-off time of 16 seconds.

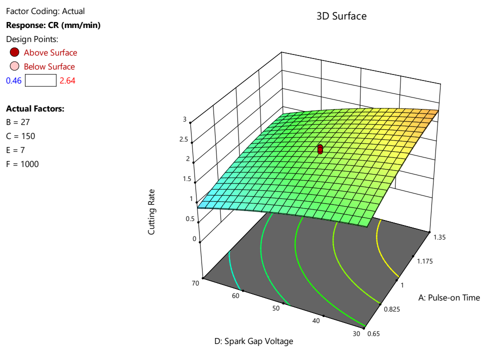


Figure 6: Response surface showing the interactive effect of pulse-on time and spark gap voltage on cutting rate at pulse-off time= 27 µs, peak current =150 A, wire running speed =7.0 m/min, and wire tension=1000 g

The response surface in figure 6 illustrates that the increase in spark gap voltage leads to the decrease in the cutting rate but the decrease is steeper at higher value of pulse-on time. The spark gap voltage determines the gap between the work piece and the wire electrode. The higher the spark gap voltage, the higher will be the gap between wire and work piece. This increases the dielectric strength of the medium and as the open circuit voltage of the machine is fixed, the discharge current during machining decreases, resulting in less melting and evaporation of the work material. As a result, the cutting rate is decreased. The spark gap voltage in the range of 30–40 V is suitable for obtaining maximum cutting rate at higher values of pulse-on time (1.17–1.35 µs) in the present case.

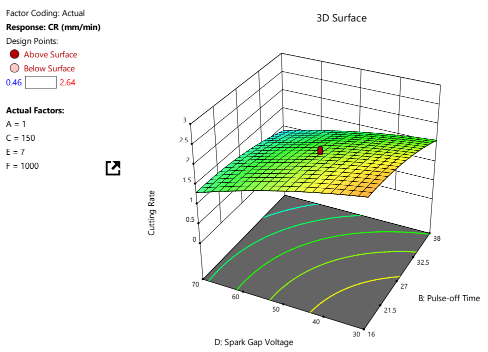


Figure 7: Response surface showing the interactive effect of pulse-off time and spark gap voltage on the cutting rate at pulse on time = 1.00 µs, peak current=150 A, wire running speed =7.0 m/min, and wire tension=1000 g

The inferences already made from figure 5 and figure 6 are confirmed here in the response surface plot (figure 7) between pulse off time and spark gap voltage.

### 5.3.2 Effect of parametric interactions on surface roughness

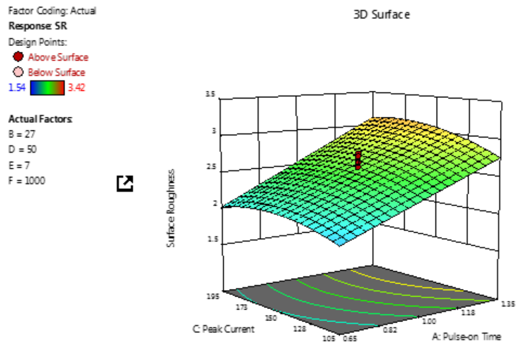


Figure 8: Response surface showing the interactive effect of pulse-on time and peak current on surface roughness at pulse-off time = 27.00 µs, spark gap voltage = 50 V, wire running speed =7.0 m/min, and wire tension= 1000 g

Figure 8 shows that the lower values of pulse-on time (0.65–0.82 µs) and peak current (105–120 A) causes minimum surface roughness. It can be claimed that larger craters may form on the surface of the workpiece when pulse-on time and peak current are high due to an increase in melting and evaporation rate.

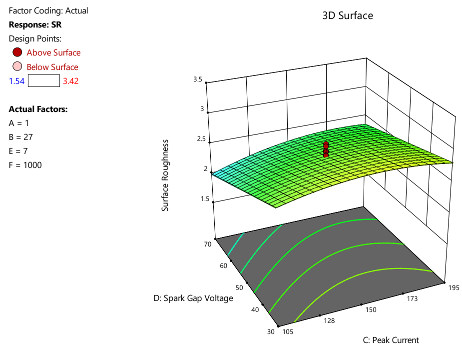


Figure 9: Response surface showing the interactive effect of peak current and spark gap voltage on surface roughness at pulse-on time= 1.00 µs, pulse-off time= 27.00 µs, wire running speed = 7 m/min, and wire tension= 1000 g

It is observed from figure 9 that lower values of peak current (105–115A) and higher values of spark gap voltage (60–70 V) results in minimum surface roughness. It may be due to fact that at the higher spark gap voltage, the gap between the wire and workpiece will widen. The discharge current decreases that lead to less melting of work material. This causes decrease in surface roughness.

### 5.3.3 Comparison of Proposed model with Previous Models

This section emphasizes the effectiveness of the proposed model by comparing it with the outcomes of existing methodologies and illustrating their outcomes based on several metrics. The comparisons are made with the previous techniques on the basis of the degrees of freedom (DF), sum of squares (SS), mean square (MS), F-ratio, and PCR%. Comparisons are made with the existing techniques such as grinding wheels (GW), cryogenic holding times (HT), and depth of cut (DOC) (Kara et al., 2020).

Figure 10 represents the comparison of degrees of freedom (DF) of the proposed model with existing techniques such as GW, HT, and DOC. Whereas the comparison of degrees of freedom attains a maximum value of GW, HT, DOC are 1.00, 2.00, 2.00 and the proposed system attains a maximum value of 3.00. The proposed model attains a high value of degrees of freedom when compared to existing techniques even though the number of nodes gets increased. As a result, it is noticed that the proposed system has high degrees of freedom because of the Response Surface Methodology (RSM)-Inconel 706.

Figure 11 represents the comparison of the sum of squares (SS) of the proposed model with existing techniques such as GW, HT, and DOC. Whereas the comparison of the sum of squares attains a maximum value of GW, HT, and DOC are 2.04, 0.3, 0.1 and the proposed system attains the maximum value of 0.1. The proposed model attains a low value of the sum of squares when compared to existing techniques even though the number of nodes decreases.

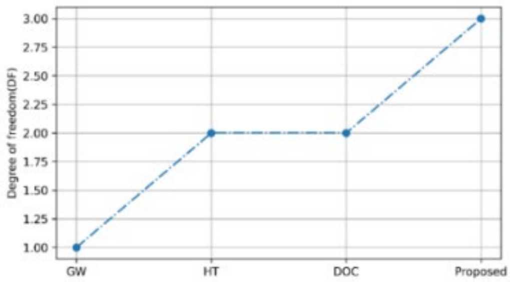


Figure 10: Comparison of Degrees of freedom (DF)

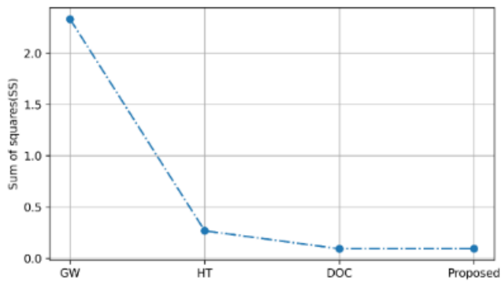


Figure 11: Comparison of sum of squares (SS)

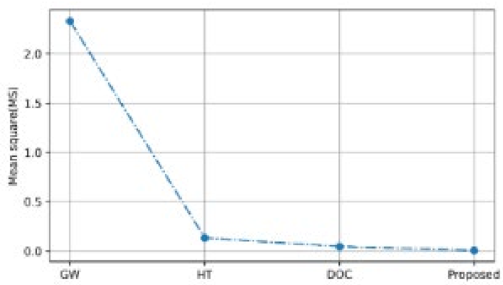


Figure 12: Comparison of Mean squares (MS)

As a result, it is noticed that the proposed system has the low sum of squares because of using Response Surface Methodology (RSM)-Inconel 706.

Figure 12 represents the comparison of mean squares (MS) of the proposed model with existing techniques such as GW, HT, DOC. Whereas the comparison of mean squares attains a maximum value of GW, HT, DOC are 2.04, 0.3, 0.1 and the proposed system attains the maximum value of 0.09. The proposed model attains a low value of mean squares when compared to existing techniques even though the number of nodes get decreased. As a result, it is noticed that the proposed system has the low mean squares because of the utilization of WEDM machining tool

Figure 13 represents the comparison of F ratio of the proposed model with existing techniques such as GW, HT, DOC. Whereas the comparison of F ratio attains a maximum value of GW, HT, DOC are 300, 40, 20 and the proposed system attains the maximum value of 10. The proposed model attains a low value of F ratio when compared to existing techniques even though the number of nodes get decreased. As a result, it is noticed that the proposed system has the low F ratio because of the utilization of WEDM machining tool.

Figure 14 represents the comparison of PCR% of the proposed model with existing techniques such as GW, HT, DOC. Whereas the comparison of mean squares attains a maximum value of GW, HT, DOC are 85, 10, 2 and the proposed system attains the maximum value of 2. The proposed model attains a low value of PCR when compared to existing techniques even though the number of nodes get decreased. As a result, it is noticed that the proposed system has the low PCR because of the utilization of WEDM machining tool.

Overall, the proposed model demonstrates that it is more efficient in providing the optimization of parameters on the cutting edge and surface roughness using RSM Inconel 706 with WEDM machining tool when compared to existing techniques such as GW, HT, DOC. The model presented in this study has a very high value of degrees of freedom 3.00, low value of sum of squares 0.1, low value of mean squares 0.09, low value of F ratio 10 and low value of PCR 2%.

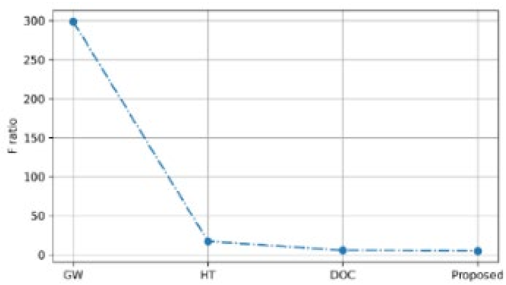


Figure 13: Comparison of F ratio

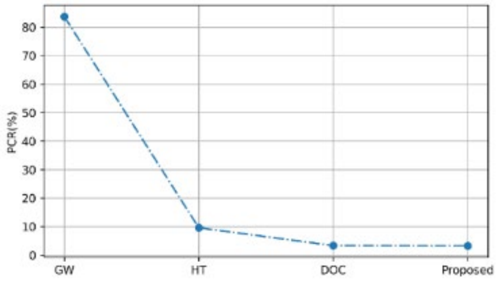


Figure 14: Comparison of PCR%

## CONCLUSIONS

The following conclusions have been made based on experimental research for machining of Inconel 706 with WEDM

1. Response surface methodology was used to create the empirical models for cutting rate and surface roughness of Inconel 706 machined by WEDM process, which are provided below

$$Cutting\ rate = -1.45023 + 3.88921 \times T_{on} + 0.027986 \times T_{off} + 0.022150 \times IP + 0.004260 \times SV - 0.001152 \times WT - 0.010888 \times T_{on} \times T_{off} - 0.011004 \times T_{on} \times IP - +0.000342 \times T_{off} \times SV - 1.09772 \times T^2{}_{on} - 0.001114 \times T^2{}_{off} - 0.000067 \times IP^2 - 0.000236 \times SV^2 + 5.63722\ E - 07 \times WT2$$

$$Surface\ roughness = 1.32684 + 0.560118 \times T_{on} - 0.005187 \times T_{off} + 0.020275 \times IP - 0.034630 \times SV + 0.003420 \times T_{on} \times IP + 0.007307 \times T_{on} \times SV + 0.000075 \times IP \times SV - 0.000083 \times IP^2$$

2. The prediction errors are within the acceptable range of ±5% consequently, consequently the empirical models for cutting rate and surface roughness for WEDM of Inconel 706 are accurate representation of the experimental findings. According to estimates, the standard uncertainty for cutting rate and surface roughness is 1.98 and 2.76%, respectively.
3. The spark gap voltage is the most influencing factor for cutting rate whereas pulse-on time is the most significant factor for surface roughness of Inconel 706. However, the peak current is not particularly important for WEDM of Inconel 706. For both cutting rate and surface roughness, wire running speed and wire tension are not significant variables.
4. The cutting rate is most significantly influenced by spark gap voltage (43.78%), followed by pulse-on time (20.87%) and pulse-off time (18.65%). The spark gap voltage's interactions with the pulse-on time and pulse-off time significantly influences the cutting rate. The pulse-on time and pulse-off time also interact strongly for cutting rate. The cutting rate rises with longer pulse-on time while it falls with longer pulse-off times and higher spark gap voltage. 2.64 mm/min has been recorded as the fastest cutting speed for Inconel 706.
5. With contributions of 63.50% and 26.73%, respectively, the spark gap voltage and pulse-on time are the main factors impacting surface roughness. Peak current and spark gap voltage strongly interact with the pulse-on time for surface roughness. The peak current interacts strongly with spark gap voltage for surface roughness. Surface roughness increases with the increase in pulse-on time and decreases with the increase in spark gap voltage. The lowest surface roughness that has been achieved is 1.54 µm.
6. Highest cutting rate of 1.88 mm/min and lowest surface roughness of 2.21 µm were obtained by the multi-response optimization by giving equal weightage to both cutting rate and surface roughness.
7. The wire running speed and wire tension have been found to be insignificant factors for both the responses.
8. Overall, the proposed model demonstrates that it is more efficient in providing the optimization of parameters on the cutting rate and surface roughness using RSM Inconel 706 with WEDM machining tool when compared to existing techniques such as GW, HT, DOC. The model presented in this study has a very high value of degrees of freedom 3.00, low value of sum of squares 0.1, low value of mean squares 0.09, low value of F ratio 10 and low value of PCR 2%.

## REFERENCES

Abhilash, P.M. and Chakradhar, D., "Effect of wire material and discharge energy on productivity and surface integrity of WEDM-processed Inconel 718," *Advances in Materials and Processing Technologies*, Vol. 8, No. 4, pp. 4698-4719, (2022).

Ahmed, B.A., "Parametric Analysis of Surface Roughness and Metal Removal Rate during Electrical Discharge Machining of O1 Tool Steel," *Journal of Engineering*, Vol. 29, No. 5, pp.115-125, (2023).

Benedict, G.F., "Electrical discharge wire cutting (EDWC)," *In: Nontraditional manufacturing* *processes, Marcel Dekker, New York*, pp 231–246, (1987).

Boopathi, S., Lewise, K.A.S., Subbiah, R. and Sivaraman, G., "Near-dry wire-cut electrical discharge machining process using water–air-mist dielectric fluid: An experimental study," *Materials Today: Proceedings*, Vol. 49, pp.1885-1890, (2022).

Dayakar, K., Raju, K.K. and Raju, C.R.B., "Prediction and optimization of surface roughness and MRR in wire EDM of maraging steel 350," *Materials Today: Proceedings*, Vol. 18, pp. 2123-2131, (2019).

Farooq, M.U., Anwar, S., Kumar, M.S., AlFaify, A., Ali, M.A., Kumar, R. and Haber, R., "A Novel Flushing Mechanism to Minimize Roughness and Dimensional Errors during Wire Electric Discharge Machining of Complex Profiles on Inconel 718," *Materials*, Vol. 15, No. 20, pp.7330, (2022).

Ho, K.H., Newman, S.T., Rahimifard, S., Allen, R.D., "State of the art in wire electrical discharge machining (WEDM)," *Int J Mach Tool Manuf.,* Vol. 44, pp. 1247–1259, (2004).

Ishfaq, K., Zahoor, S., Khan, S.A., Rehman, M., Alfaify, A. and Anwar, S., "Minimizing the corner errors (top and bottom) at optimized cutting rate and surface finish during WEDM of Al6061," *Engineering Science and Technology, an International Journal*, Vol. 24, No. 4, pp.1027-1041, 2021.

Kalpakjian, S., Schmid, S.R., "Material-removal processes: abrasive, chemical, electrical, and high-energy beams," *In: Manufacturing processes for engineering materials, 5th edn. Pearson Education*, pp 561–565, (2008).

Kara, F., Köklü, U. and Kabasakaloğlu, U., "Taguchi optimization of surface roughness in grinding of cryogenically treated AISI 5140 steel," *Materials Testing*, Vol. 62, No. 10, pp. 1041-1047, (2020).

Khatri, P.N.J.D.B., "parametric study and experimental investigation of material removal capability of powder mixed electric discharge machining,"

Kinoshita, N., Fukui, M., Gamo, G., "Control of wire-EDM preventing electrode from breaking," *CIRP Ann Manuf Technol*., Vol. 31, pp. 111–114, (1982).

Kumarswamy, Y., Ganesh, P.D., Kumar, K.R., Varun, S.S., Vamsi, G.J. and Phaneendra, Y., "Optimize the process parameters of wire EDM and to analyse the welding characteristics of tig welding joints using AISI 308," In *E3S Web of Conferences*. *EDP Sciences*, Vol. 391, pp. 01043, (2023).

Manoj, I.V., Soni, H., Narendranath, S., Mashinini, P.M. and Kara, F., "Examination of machining parameters and prediction of cutting velocity and surface roughness using RSM and ANN using WEDM of Altemp HX," *Advances in Materials Science and Engineering*, pp.1-9, (2022).

Pandey, P.C., Shan, H.S., "Thermal metal removal processes," *In: Modern machining processes. Tata McGraw-Hill Education*, pp. 84–113, (2010).

Pawar, P.J. and Khalkar, M.Y., "Multi-objective optimization of wire-electric discharge machining process using multi-objective artificial bee colony algorithm," In *Advanced Engineering Optimization Through Intelligent Techniques: Select Proceedings of AEOTIT 2018*. *Springer Singapore,* pp. 39-46, (2020).

Perumal, A., Kailasanathan, C., Stalin, B., Suresh Kumar, S., Rajkumar, P.R., Gangadharan, T., Venkatesan, G., Nagaprasad, N., Dhinakaran, V. and Krishnaraj, R., "Multiresponse optimization of wire electrical discharge machining parameters for Ti-6Al-2Sn-4Zr-2Mo (α-β) alloy using taguchi-grey relational approach," *Advances in Materials Science and Engineering*, pp.1-13, (2022).

Prajapati, K.J., Bhuva, B.V., Patel, V.D. and Patel, M.B., "A Review-Parametric Optimization of Process Parameter for Electro Discharge Machining of Inconel alloy," (2022).

Saha, S., Maity, S.R. and Dey, S., "Comparative Analysis of Metaheuristic Optimizers in the Performance Optimization of Wire Electric Discharge Machining Processes," *Operational Research in Engineering Sciences: Theory and Applications*, Vol. 6, No. 1, (2023).

Scott, D., Boyina, S., Rajurkar, K.P., "Analysis and optimization of parameter combinations in wire electrical discharge machining," *Int J Prod Res.,* Vol. 29, pp. 2189–2207, (1991).

Sharman, A.R.C., Hughes, J.I., Ridgway, K., "An analysis of the residual stresses generated in Inconel 718TM when turning," *J Mater Process Technol*., Vol. 173, pp. 359–367, (2006).

Shaw, M.C., Nakayama, K., "Machining high strength materials," *CIRP Ann*., Vol. 15, pp. 45–59, (1967).

Thakur, D.G., Ramamoorthy, B., Vijayaraghavan, L., "Study on the machinability characteristics of superalloy Inconel 718 during high speed turning," *Mater Des.,* Vol. 30, pp. 1718–1725, (2009).

Thomas, A., El-Wahabi, M., Cabrera, J.M., Prado, J.M., "High temperature deformation of Inconel 718," *J Mater Process Technol.,* Vol. 177, pp. 469–472, (2006).

Wang, Z.Y., Rajurkar, K.P., Fan, J., Lei, S., Shin, Y.C., Petrescu, G., "Hybrid machining of Inconel 718," *Int J Mach Tool Manuf.,* Vol. 43, pp. 1391–1396, (2003).

Williams, R.E., Rajurkar, K.P., "Study of wire electrical discharge machined surface characteristics," *J Mater Process Technol*., Vol. 28, pp. 127–138, (1991).

## Appendix-I
## ANOVA for Reduced Quadratic model

### Response 1: Cutting Rate

| Source | Sum of Squares | df | Mean Square | F-value | p-value | - |
|---|---|---|---|---|---|---|
| **Model** | 15.76 | 13 | 1.21 | 139.90 | < 0.0001 | significant |
| A-A | 3.29 | 1 | 3.29 | 379.67 | < 0.0001 | - |
| B-B | 2.94 | 1 | 2.94 | 339.27 | < 0.0001 | - |
| C-C | 0.3335 | 1 | 0.3335 | 38.50 | < 0.0001 | - |
| D-D | 6.90 | 1 | 6.90 | 796.49 | < 0.0001 | - |
| F-F | 0.0034 | 1 | 0.0034 | 0.3889 | 0.5366 | - |
| AB | 0.0553 | 1 | 0.0553 | 6.38 | 0.0158 | - |
| AD | 0.2000 | 1 | 0.2000 | 23.09 | < 0.0001 | - |
| BD | 0.1845 | 1 | 0.1845 | 21.30 | < 0.0001 | - |
| $A^2$ | 0.2569 | 1 | 0.2569 | 29.65 | < 0.0001 | - |
| $B^2$ | 0.2417 | 1 | 0.2417 | 27.89 | < 0.0001 | - |
| $C^2$ | 0.2492 | 1 | 0.2492 | 28.77 | < 0.0001 | - |
| $D^2$ | 0.1365 | 1 | 0.1365 | 15.76 | 0.0003 | - |
| $F^2$ | 0.0960 | 1 | 0.0960 | 11.08 | 0.0020 | - |
| **Residual** | 0.3292 | 38 | 0.0087 | | | - |
| Lack of Fit | 0.3084 | 31 | 0.0099 | 3.35 | 0.0508 | not significant |
| Pure Error | 0.0208 | 7 | 0.0030 | | | - |
| **Cor Total** | 16.09 | 51 | | | | - |

### Fit Statistics

| | | | |
|---|---|---|---|
| **Std. Dev.** | 0.0931 | **$R^2$** | 0.9795 |
| **Mean** | 1.46 | **Adjusted $R^2$** | 0.9725 |
| **C.V. %** | 6.37 | **Predicted $R^2$** | 0.9608 |
| - | - | **Adeq Precision** | 46.2929 |

## Appendix-II
## ANOVA for Reduced Quadratic model

### Response 2: Surface Roughness

| Source | Sum of Squares | df | Mean Square | F-value | p-value | |
|---|---|---|---|---|---|---|
| **Model** | 14.85 | 8 | 1.86 | 90.54 | < 0.0001 | significant |
| A-A | 9.43 | 1 | 9.43 | 459.73 | < 0.0001 | |
| B-B | 0.1171 | 1 | 0.1171 | 5.71 | 0.0213 | |
| C-C | 0.5184 | 1 | 0.5184 | 25.28 | < 0.0001 | |
| D-D | 3.97 | 1 | 3.97 | 193.67 | < 0.0001 | |
| AC | 0.0925 | 1 | 0.0925 | 4.51 | 0.0395 | |
| AD | 0.0882 | 1 | 0.0882 | 4.30 | 0.0441 | |
| CD | 0.1513 | 1 | 0.1513 | 7.38 | 0.0095 | |
| $C^2$ | 0.4873 | 1 | 0.4873 | 23.76 | < 0.0001 | |
| **Residual** | 0.8819 | 43 | 0.0205 | | | |
| Lack of Fit | 0.8092 | 36 | 0.0225 | 2.16 | 0.1447 | not significant |
| Pure Error | 0.0727 | 7 | 0.0104 | | | |
| **Cor Total** | 15.74 | 51 | | | | |

### Fit Statistics

| | | | |
|---|---|---|---|
| **Std. Dev.** | 0.1432 | **$R^2$** | 0.9440 |
| **Mean** | 2.52 | **Adjusted $R^2$** | 0.9335 |
| **C.V. %** | 5.68 | **Predicted $R^2$** | 0.9170 |
| | | **Adeq Precision** | 34.1145 |